ELSEVIER

Applied Ocean Research 21 (1999) 113–125

Applied Ocean Research

The motion of a rigid body impelled by sea-wave impact

S.J. Cox*, M.J. Cooker

School of Mathematics, University of East Anglia, Norwich, NR4 7TJ, UK

Received 24 November 1998; accepted 10 March 1999

Abstract

A wave breaking against a sea wall causes high pressure gradients to act along the sea bed, pushing objects away from the wall. This situation is modelled using pressure impulse theory to show that, for a large object near a sea wall, the impulsive force due to the wave will move the object. This force can be found, given knowledge of the added mass and volume of an object. In particular, if the wall is thought of as a plane, gently sloping beach, then this theory may explain how shingle beaches are graded according to the size of the shingle, with larger boulders being moved farthest by the impact of a wave. In order to obtain estimates for the distances moved up, or down, the beach, a single boulder is treated as a spherical body which is free to move.

Keywords: Beach material sorting; Breaking waves; Impulsive motion; Wave impact pressures

1. Introduction

In this paper we consider the consequences of a water wave breaking violently on a beach or against a sea wall. The key characteristic of this kind of flow is that the fluid velocity everywhere undergoes a finite change during a short time interval. This velocity change causes an impulsive fluid force on a rigid body in the fluid, which depends on the body's volume and shape and the degree to which it is free to move. We predict that this wave impact force may be great enough to overcome the natural forces which normally anchor a body in place. It could help to explain how breakwaters are damaged by wave impact and how boulders are moved around during storms.

The high pressures which are generated when a large sea wave enters shoaling water and breaks can cause breakwaters to fail. This often happens because the wave forces on the breakwater caissons cause them to slide out of position. The largest caisson movements occur during storms, when the waves are higher, steeper and more frequent. At Sakata Port in Japan, during the winter of 1973/74, the breakwater failed due to sliding of the caissons. Tanimoto and Takahashi [1] record the sliding distances of 8 m high caissons due to the impact of large waves, showing movements of almost 4 m away from their initial position. Similar damage occurred at Mutsu–Ogawara Port in Japan [2].

Laboratory data suggests that the highest wave impact pressures are associated with waves that trap only a small amount of air as they break against a wall [3]. The pressure rises to its peak, p_{peak}, and falls back to near hydrostatic pressure over a short time Δt. The value of Δt may be estimated in any of a number of ways, though its precise value is relatively unimportant in the following analysis. A range or statistical distribution of values might be appropriate, but here we take Δt to be about 1×10^{-2} s. If the depth of water at the wall is $H = 10$ m then the speed of the wave is $u_0 = \sqrt{gH} \approx 10\ \text{m s}^{-1}$. Corresponding peak pressures are $p_{\text{peak}} = 5 \times 10^4\ \text{N m}^{-2}$ [3,4]. However, for apparently identical incident wave conditions these values can vary markedly [5], but Bagnold [6] found that, whilst the peak pressure varied, the product $(1/2)p_{\text{peak}}\Delta t$ remained fairly constant.

Consider a cubic caisson of side $h = 8$ m and density $\rho_B = 3 \times 10^3\ \text{kg m}^{-3}$. Its wet weight is $F_W \approx 1 \times 10^7$ N. We take a coefficient of friction of $\mu = 1/2$ between the caisson and the bed, and then the frictional force holding the caisson in place is $F_F = 5 \times 10^6$ N. There are three 'pressure' forces acting on the side of the caisson, trying to move it:

- The hydrostatic pressure force, due to the depth of water at the wall: $F_H \sim (1/2)\rho g h^3 \approx 2.5 \times 10^6$ N, where ρ is the density of the water.
- The fluid drag, F_D, exerted by the liquid flowing over the caisson, due to the passage of the waves. We take $F_D = 1/2\rho C_D u_0^2 h^2$ where C_D is a drag coefficient at

* Corresponding author. Present address: Department of Physics, Trinity College, Dublin 2, Ireland.

E-mail addresses: coxs@tcd.ie (S.J. Cox), m.cooker@uea.ac.uk (M.J. Cooker)

0141-1187/99/$ - see front matter
PII: S0141-1187(99)00005-X

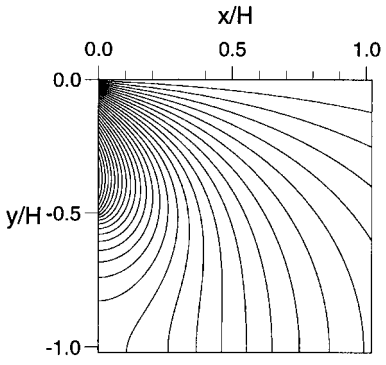

Fig. 1. Lines of constant pressure impulse for a wave impacting against the top half of the wall, $x = 0$, $y \in [-0.5H, 0]$, with a uniform impact velocity. Contour separation is $0.01\rho u_0 H$.

approximately constant flow speed (appropriate to the Reynolds number). Putting $C_D = 1/2$ implies that $F_D \approx 1 \times 10^6$ N.

- The impulsive pressure force, F_I, due to the rapid change in fluid velocity. We will find that $F_I \sim \rho u_0 h^3/\Delta t \approx 5 \times 10^8$ N.

Then the impulsive pressure force exceeds all the others by at least an order of magnitude and is the only one able to overcome the frictional force and move the caisson. So in the region where waves are breaking, and during the brief time of impact, we expect this impulsive pressure force to be the dominant mechanism for moving objects around. In particular, it is likely to move armour units from their position at the base of a breakwater. These can cause damage to the wall in one of two ways: either directly, by solid body impact, or inadvertently, since by their absence waves are able to break with more force against the wall. This is illustrated by the damage to the Sines breakwater in Portugal [7], which occurred in 1978. The breakwater failed due to the movement and loss of the 'dolos' armour units—those units that broke free then proceeded to batter the wall further. Further observations of impulsive forces include blocks of stone of a hundred tons in weight having been disturbed by heavy seas [8]. Gaillard [9, Section 8] gives many instances of the destructive forces exerted by waves, including that of a 20 ton block being lifted vertically to land atop a pier of 12 feet in height, almost 5 feet above the level of high water.

Our work also applies to the movement of large boulders by wave impact. Stevenson [10] observed the "remarkable destructive effects at Whalsey Skerries" in Scotland, where "blocks of 6 tons weight have been quarried or broken out of their beds in situ… [by]aqueous action". He also records the passage of a rock, weighing seven and a half tons, across 73 feet of rugged ledges, at a height of 20 feet above the sea. This feat is remarkable, even if we assume that it occurred in many small successive motions over a long period of time. These events also occur in smaller expanses of water, for instance in the great lakes of America, where Stevenson [11] quotes observations of stones "weighing upwards of half-a-ton [being] completely turned over".

At the instant of impact, there is a distribution of peak pressure throughout the fluid. Grilli et al. [12] inserted eight pressure sensors on the bed of a laboratory tank, close to the base of a vertical wall against which waves were made to break. They found that large impact pressures were recorded at a considerable distance from the wall and that these pressures propagated very rapidly. Moreover, there were pressure gradients along the bed, away from the wall with magnitudes of up to about $2\rho g$, where g is the acceleration due to gravity. Müller [13] performed small-scale experiments on waves breaking against a vertical wall and found pressure gradients away from the wall of up to almost $8\rho g$. The impulsive pressure gradient causes an impulsive force to act on a body on the sea bed, pushing it away from the wall.

However, rather than using the peak pressure, we will describe the problem in terms of the product $P = (1/2)p_{\text{peak}}\Delta t$ which is found to remain constant for identical wave impacts even though the peak pressure and duration of impact may vary [6]. If the pressure, p, just rises to its peak value and then falls back, so that a plot of pressure versus time looks like a delta-function, we can write

$$P(x, y, z) = \int_{t_b}^{t_a} p(x, y, z, t)\, \mathrm{d}t \tag{1}$$

where t_b and t_a are the times before and after impact and P is the pressure impulse. If $\Delta t = t_a - t_b$ is small enough then we will show that $\nabla^2 P = 0$ in the fluid domain, with mixed boundary conditions.

Cooker and Peregrine [14] calculate the pressure impulse in a fluid domain, D, whose shape resembles a sea wave at its moment of impact against a vertical wall of height H. D is the region $x \geq 0$, $-H \leq y \leq 0$, with the wall at $x = 0$ and the horizontal sea bed at $y = -H$. The distribution of P is shown in Fig. 1, in the case where the wave breaks against the top half of the wall. The wave moves in the negative x direction before impact, with constant uniform speed, u_0. The gradient of pressure impulse is normal to the contours drawn in Fig. 1. We see that there are gradients acting along the sea bed, trying to move objects away from the wall, and down the wall. These gradients are directly proportional to the finite change in flow velocity which occurs throughout the fluid domain during the impact.

We estimate a pressure impulse gradient, G, along the bed from Fig. 1: at $x/H = 0.5$ the pressure impulse gradient is $G = 0.1\rho u_0$. This is about twice as large as the pressure impulse gradients which were found experimentally by Müller [13] (a pressure gradient of $8\rho g$ translates into pressure impulse gradients of approximately $0.04\rho u_0$) and could therefore be a reasonable estimate for storm waves.

Cooker and Peregrine use their analysis [14] to supply a far-field boundary condition for the problem of finding the impulse on a body which is free to move and initially at rest on the sea bed [15]. They consider bodies such as

hemispherical boulders and circular cylinders, this latter being appropriate to parts of armour units near breakwaters. We extend their work, by giving general formulae for the impulse on, and velocity of, the body, allowing more shapes to be treated.

We shall describe pressure impulse theory and then pose a boundary-value-problem for P in the neighbourhood of a general two-dimensional body on the bed of the domain, D. Integrating $P\mathbf{n}$ over the surface of the body (where $\mathbf{n}$ is the normal to the surface of the body) allows the impulse on it to be found. In Section 3.1 the impulse on a fixed body is expressed in terms of the conformal map used to generate it. Using a Laurent expansion for the conformal map allows an alternative formulation to be made in Section 3.2, and in Section 3.3 we modify the theory for a body which is free to move. Section 3.4 shows that the impulse and velocity of a body on any solid surface, not necessarily horizontal, can be found. In Section 4 we explore in detail the impulse on several rigid body shapes on the sea bed, including a rectangular cylinder and an inclined plate. In Section 5 we treat the case of a three-dimensional boulder moving across the surface of a beach, which is subjected to gravity, buoyancy, friction and fluid drag, as well as the impulsive fluid force due to a nearby wave impact. The boulder's shape is not specific to the substance of the model equations, but for simplicity we choose a spherical boulder. The model shows that a larger boulder is pushed further up the beach than a small boulder. A succession of wave impacts might push the body along in a succession of short steps which could sum to a considerable distance over the duration of a storm.

2. Pressure impulse theory

Over the duration of the impact, we distinguish a velocity field before impact, $\mathbf{u}_b$, from a quite distinct velocity field after impact, $\mathbf{u}_a$. Whilst $\mathbf{u}_b$ and $\mathbf{u}_a$ may vary in time, we suppose that during the short period of time of impact, the acceleration of the fluid, $\partial\mathbf{u}/\partial t$, greatly exceeds its value at all other times. This acceleration is associated with a large pressure gradient and has striking consequences for the equations of motion. We neglect viscosity and then Euler's equations are

$$\frac{\partial \mathbf{u}}{\partial t} + (\mathbf{u}\cdot\nabla)\mathbf{u} = -\frac{1}{\rho}\nabla p - g\mathbf{k} \tag{2}$$

where $\mathbf{u}$ is the velocity, p the pressure and ρ the density of the fluid, g is the acceleration due to gravity and $\mathbf{k}$ is a unit vector pointing vertically up. We non-dimensionalise the variables with a time scale Δt, a length scale L, a velocity scale u_0 and a pressure scale p_0. The length scale L is associated with the depth of water prior to the impact and u_0 is pertinent to the speed of waves approaching the wall. Then, after some manipulation, with primes denoting dimensionless variables,

$$\frac{\partial \mathbf{u}'}{\partial t'} + S(\mathbf{u}'\cdot\nabla')\mathbf{u}' = -\frac{\Delta t p_0}{\rho u_0 L}\nabla' p' - \frac{\Delta t}{u_0} g\mathbf{k} \tag{3}$$

where $S = \Delta t u_0/L$. Typically, if $L \sim 10$ m, $u_0 \sim 10$ m s^{-1} and $\Delta t \sim 0.01$ s then $S = 0.01$ and the quantity scaling gravity is 0.001. So we seek a balance between the first term and the pressure term in Eq. (3) by scaling pressure according to $p_0 = \rho u_0 L/\Delta t$, which is very large ($1 \times 10^7$ N m^{-2}). Since they are small compared to unity, we neglect the non-linear convective terms and the last term in Eq. (3). Now Eq. (2) becomes (in dimensional variables)

$$\frac{\partial \mathbf{u}}{\partial t} = -\frac{1}{\rho}\nabla p. \tag{4}$$

Integrating Eq. (2) with respect to time over the short duration of the impact, $\Delta t = t_a - t_b$ gives

$$\mathbf{u}_a - \mathbf{u}_b = -\frac{1}{\rho}\nabla P \tag{5}$$

where

$$P(x,y) = \int_{t_b}^{t_a} p(x,y,t)\,\mathrm{d}t \tag{6}$$

is the pressure impulse. If the pressure rises to p_{peak} and then falls we have

$$P \approx \frac{1}{2} p_{peak}\Delta t \text{ or, alternatively, } p_{peak} \approx \frac{2P}{\Delta t} \tag{7}$$

so that we can use the knowledge gained about P to estimate corresponding peak pressures. We assume that the fluid is incompressible before impact and after impact, $\nabla\cdot\mathbf{u}_b = 0$ and $\nabla\cdot\mathbf{u}_a = 0$, and suggest that fluid compressibility may be accommodated through modifying Eq. (7), by altering Δt for instance.

Then the divergence of Eq. (5) shows that P satisfies Laplace's equation,

$$\nabla^2 P = 0. \tag{8}$$

Eq. (8) is independent of time, and we solve it in the fluid domain at the start of the impact. We can provide appropriate Neumann or Dirichlet boundary conditions to solve for P in one of four forms:

- $\nabla P\cdot\mathbf{n} = 0$ on a fixed impermeable surface (with normal vector $\mathbf{n}$) which is in contact with the fluid before and after impact. That is, fluid cannot pass through the boundary.
- $\partial P/\partial n = \rho\mathbf{u}_b\cdot\mathbf{n}$ where fluid impacts on a solid surface with velocity $\mathbf{u}_b$ and remains in contact with the surface after impact (whence $\mathbf{u}_a\cdot\mathbf{n} = 0$). This is a consequence of Eq. (5).
- P or ∇P specified in the far field.
- $P = 0$ on a free surface. Since pressure, p, is constant on a free surface, we can define P up to an arbitrary constant, and without loss of generality this constant is zero. A

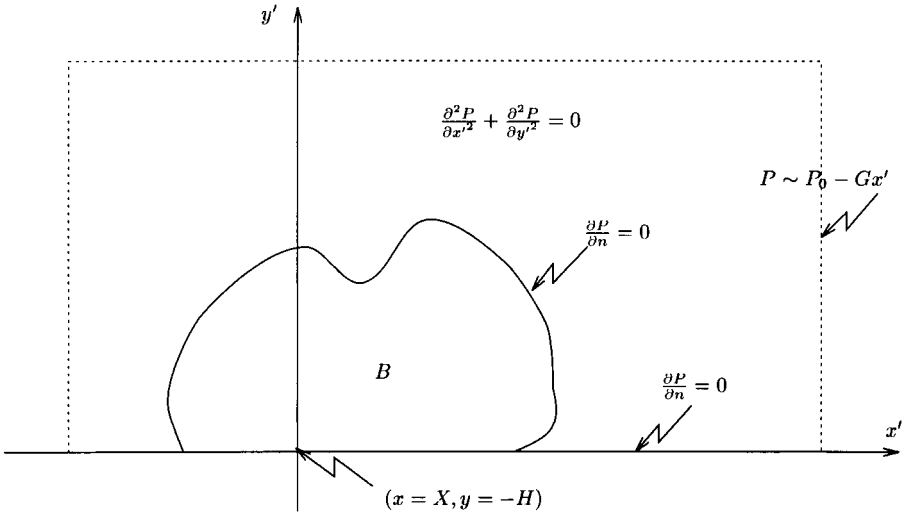

Fig. 2. The boundary-value-problem for the pressure impulse P. The free surface lies far off in the y' direction and the base of the wall is far off in the negative x' direction. P satisfies Laplace's equation and the far field condition (dotted line) is that $P \sim P_0 - Gx'$. For a body at rest, the normal velocity is zero on both B and the sea bed, $y = -H$.

consequence of this is that we can take any contour of constant pressure impulse to be a free surface for the flow.

As well as giving information on peak pressures, knowledge of P will determine the velocity field after impact through Eq. (5). Notice also that the curl of Eq. (5) shows that the vorticity is the same before and after impact.

We proceed by taking a field of pressure impulse, P_1, which has already been calculated, and finding the change in P_1 brought about by the presence of a rigid body, B, at rest on the bed of the fluid domain, D. By considering B much smaller than the significant length scale in D, it is reasonable to suppose that the effect of B on P_1 is confined to a region near B. For example, a semicircle, B, of radius a, can be placed on the bed of the rectangular domain described above provided $a \ll H$. The centre of B is at $x = X, y = -H$, and then $\partial P_1/\partial x|_{x=X,y=-H} = -G$ is evaluated. From now on, G is treated as a constant for the purposes of the flow in the neighbourhood of B. Also constant is $P_1|_{x=X,y=-H} = P_0$. These two conditions can be combined to give a condition on the distorted pressure impulse field

$$P(x,y) \sim P_0 - Gx \tag{9}$$

which is to be satisfied in the far field of the model for flow around B. Usually, Eq. (9) is achieved within a few radii of B (notice how nearly parallel the contours in Fig. 1 are in a region close to the sea bed around $x/H = 0.5$), and so the whole of the model near B lies in a region whose dimensions are small compared with H. The pressure impulse near B satisfies the boundary-value-problem shown in Fig. 2. New coordinates $x' = x - X, y' = y - (-H)$ are introduced and the bed boundary condition changes to $\partial P/\partial n = 0$ on both the boundary of B and the remainder of the bed. P continues to satisfy Laplace's equation and the far field boundary condition Eq. (9). More generally, x' could be a coordinate indicating arc length along a solid surface and y' normal to the surface. (The far field condition might also be directly proportional to y' if B lay inside an impact zone. Approximations of order higher than those in Eq. (9) can be calculated, but the term proportional to the square of x' has no net effect on the impulse for a left–right symmetric body.) The boundary condition on B significantly changes the pressure impulse contours near the bed, usually attracting them towards B and thereby increasing the impulse on the body.

3. Mathematical formulation

Given P_0 and G, we will find that the presence of a body, B, causes a distortion to the pressure impulse, P. The real axis of a w plane will be conformally mapped to a physical sea bed in a z plane. The map will generate a body in the form of a simple geometric shape on a horizontal base with an explicit transformation in the form $z = z(w)$, from either the upper half-plane or the exterior of the unit circle. Examples of such maps are given by Kober [16].

Consider an arbitrary body $\bar{B}$ with boundary $\partial\bar{B}$ in an infinite fluid. We define a 'complex pressure impulse' (CPI), $\Phi: \mathbb{C} \to \mathbb{C}$ by $\Phi(z) = P(x,y) + \mathrm{i}Q(x,y)$, where $\mathrm{i} = \sqrt{-1}$, $z = x + \mathrm{i}y$, P is pressure impulse and Q is defined, up to an arbitrary constant, by the Cauchy–Riemann equations:

$$\frac{\partial P}{\partial x} = \frac{\partial Q}{\partial y}, \qquad \frac{\partial P}{\partial y} = -\frac{\partial Q}{\partial x}.$$

Since the lines of constant Q are perpendicular to the lines of constant pressure impulse, Q is constant on $\partial\bar{B}$ (without loss of generality $Q = 0$).

The conformal transformation, $z = z(w)$, maps the

complex $w = u + iv$ plane to the complex z plane containing the body $\bar{B}$. The real axis in the w plane, $v = 0$, is mapped to the union of the sea bed on either side of $\bar{B}$, $y = 0$, and $\partial\bar{B}$. The pre-image of $\partial\bar{B}$ is denoted $\partial\bar{B}'$, lying along the real w-axis between $u = u_1$ and $u = u_2$. Pressure impulse contours in the w plane (lines of constant u) are mapped to pressure impulse contours around $\bar{B}$. If the map is such that $z \sim \sigma w$ as $|z| \to \infty$, for some constant $\sigma > 0$, then in the w plane the CPI is $\Phi(w) = P_0 - G\sigma w$ and $\Phi(z) = P_0 - G\sigma w(z) \sim P_0 - Gz$ as $|z| \to \infty$.

3.1. The impulse on B

Let a small segment of $\partial\bar{B}$ be denoted ds and the angle between the tangent to $\bar{B}$ and the positive real axis be ϕ. The impulse on $\bar{B}$ has horizontal and vertical components given by $\bar{\mathbf{I}} = (\bar{I}_x, \bar{I}_y)$ where

$$\bar{I}_x + i\bar{I}_y = \int_{\partial\bar{B}} P(z) \sin\phi \, ds - i \int_{\partial\bar{B}} P(z) \cos\phi \, ds \tag{10}$$

$$= -i \int_{\partial\bar{B}} (P + iQ)(\cos\phi + i\sin\phi) \, ds \tag{11}$$

$$= -i \int_{\partial\bar{B}} \Phi(z) dz \tag{12}$$

since $dz = e^{i\phi} ds$. These formulae hold when $\partial\bar{B}$ is a closed curve. If $\bar{B}$, and therefore $\partial\bar{B}$, has the real axis as its line of symmetry then the body B in which we are interested is the top half of $\bar{B}$, projecting above the real axis. $\partial P/\partial y = 0$ on the real axis, so the horizontal impulse, I_x, on the body B projecting into the upper half-plane is half that on $\bar{B}$. We write this impulse on B as $\mathbf{I} = (I_x, I_y)$. In which case we can perform the integration along a path in the w plane so that Eq. (12) becomes

$$I_x + iI_y = -i \int_{\partial\bar{B}'} \Phi(w) \frac{dz}{dw} \, dw \tag{13}$$

$$= -i \int_{u_1}^{u_2} (P_0 - G\sigma u) \frac{dz}{dw}\Big|_{w=u} du \tag{14}$$

$$= -iP_0(z(u_2) - z(u_1)) + iG\sigma(u_2 z(u_2) - u_1 z(u_1)) - iG\sigma \int_{u_1}^{u_2} z(u) \, du. \tag{15}$$

The first term of Eq. (15) is a vertical (downward) impulse equal to P_0, the local pressure impulse, multiplied by the length of the body along the x-axis. We assume that a body which has a flat base and is free to move will have a thin layer of fluid, of constant width, beneath it [15] (otherwise we are led into a consideration of frictional forces which we make no attempt to model, such as the stickiness of mud etc., and a requirement that we modify the normal reaction force of the bed on B, and hence the frictional force). Then the impulse generated by this fluid is also P_0 multiplied (at least in two-dimensional analysis) by the length of the base, but in an upward direction. So we conclude that this vertical impulse has no effect on the subsequent sliding motion of the object.

The second term of Eq. (15) is zero for left–right symmetric bodies. By integrating the third term in Eq. (15) we can find the total impulse on B. Now u_1, u_2, $z(u_1)$ and $z(u_2)$ are real, so this term is the only one that could possibly give a real component in Eq. (15), contributing to a horizontal component of impulse. If the body is symmetric then $u_1 = -u_2$ and we expect the integral to be purely imaginary. Thus for left–right symmetric bodies, Eq. (15) becomes

$$I_x = -iG\sigma \int_{-u_2}^{u_2} z(u) \, du \qquad \text{and} \qquad I_y = -2z(u_2)P_0. \tag{16}$$

If the conformal map is given in the form $dz/dw = f(w)$ we perform the integration in Eq. (14) and take real and imaginary parts to find the horizontal and vertical components of impulse respectively.

If the body is free to move then we can also find its initial velocity. We next derive some methods to allow straightforward calculation of the impulse and velocity.

3.2. Laurent expansion

An easier way of calculating the horizontal impulse is to use a Laurent series to represent the conformal map, as follows. If $\partial\bar{B}$ is a simple closed curve surrounded by fluid, with the point $z = 0$ inside $\partial\bar{B}$ and $\int_{\partial\bar{B}} z dz = 0$, and if Φ can be expressed as a Laurent series, i.e.

$$\Phi = G \sum_{k=-1}^{\infty} \frac{a_k}{z^k}, \qquad a_k \in \mathbb{C} \tag{17}$$

then by Cauchy's residue theorem, with the contour traversed in a clockwise manner, Eq. (12) gives

$$\bar{I}_x = -i \cdot 2\pi i \, \mathrm{R}(-Ga_1) = -2\pi G \, \mathrm{R}(a_1) \tag{18}$$

where R denotes real part. The expansion of the conformal map, $z(w)$, as a Laurent series for large w, gives a_1. Thus, if

$$z(w) = \sigma w + b_0 + \frac{b_1}{w} + \frac{b_2}{w^2} + \cdots \tag{19}$$

we substitute $w = z/\sigma$, and then $a_1 = \sigma b_1$ and Eq. (18) becomes

$$\bar{I}_x = -2\pi G \, \mathrm{R}(\sigma b_1). \tag{20}$$

For a conformal map from the exterior of the unit circle ($|S| = 1$ in a complex S plane) to the exterior of the body $\bar{B}$ (in the z plane), we can write

$$z(S) = \sigma_1 S + c_0 + \frac{c_1}{S} + \frac{c_2}{S^2} + \cdots \tag{21}$$

with $\sigma_1 > 0$. The composition of a map from the unit circle to a flat plane with a map from the flat plane to $\bar{B}$, from Eq.

(19), is

$$z(w(S)) = z\left(S + \frac{1}{S}\right) = \sigma S + b_0 + \frac{\sigma + b_1}{S} + \cdots$$

which we compare with Eq. (21) to show that $\sigma = \sigma_1$, $b_0 = c_0$ and $b_1 = c_1 - \sigma$. Then the horizontal impulse, given by Eq. (20), is

$$\bar{I}_x = 2\pi G\sigma_1^2\left[1 - \mathrm{R}\left(\frac{c_1}{\sigma_1}\right)\right]. \tag{22}$$

Pólya [17], in his calculations of the two-dimensional motion of a solid through a fluid which is at rest at infinity, constructs the cross-section of a cylindrical body $\bar{B}$ using a conformal map, as in Eq. (21). The body, of mass per unit length m, moves as if its mass per unit length were $m + \bar{M}_x$, where $\bar{M}_x$ is the added mass per unit length of the body for motion parallel to the x-axis. Then he derives the following formula for $\bar{M}_x$:

$$\frac{\bar{M}_x}{\rho} + \mathscr{V} = 2\pi\sigma_1^2\left[1 - \mathrm{R}\left(\frac{c_1}{\sigma_1}\right)\right]$$

where $\mathscr{V}$ is the volume per unit length of the body (i.e. cross-sectional area for a two-dimensional body) and ρ is the density of the fluid. This is analogous to the result in Newman [18, Section 4.14] connecting added mass and dipole moment. Thus

$$\bar{I}_x = G\left(\frac{\bar{M}_x}{\rho} + \mathscr{V}\right). \tag{23}$$

For the body B in which we are interested, which is the upper half of a body $\bar{B}$ which has its line of symmetry along the real axis, the impulse is half that on $\bar{B}$ and the results Eqs. (20), (22) and (23) become $I_x = Gk$ where

$$k = -\pi\,\mathrm{R}(\sigma b_1) \tag{24}$$

$$k = \pi\sigma_1^2\left[1 - \mathrm{R}\left(\frac{c_1}{\sigma_1}\right)\right] \tag{25}$$

$$k = \frac{M_x}{\rho} + \mathscr{V}. \tag{26}$$

Here M_x is the added mass of B for motion in the x-direction. If the area of B is non-zero (i.e. B is not a line segment) then the added mass is proportional to the displaced mass of water. We define an added mass coefficient, λ_x, which is dependent upon the shape of $\bar{B}$ by $M_x = \lambda_x\rho\mathscr{V}$ and so

$$k = \mathscr{V}(\lambda_x + 1). \tag{27}$$

Values of λ_x are tabulated for many shapes, but in those cases where they are not, we can calculate λ_x by finding k and $\mathscr{V}$. So those shapes which receive the greatest impulse per unit area are those with the largest added mass coefficients.

3.3. A moving body

If B is free to move, then we assume that the pressure impulse gradient, G, will accelerate it from rest to a horizontal velocity, V. The boundary condition on the moving body is now $\partial P/\partial n = -\rho V\hat{\mathbf{i}}\cdot\mathbf{n}$, with the same far field condition as before, $P \sim P_0 - Gx$, and the same impermeability condition on the sea floor, $\partial P/\partial y|_{y=0} = 0$. The pressure impulse which satisfies these conditions is $P_1 = \hat{P} - \rho Vx$ where $\hat{P}$ is the same as P for a fixed body but with the effective pressure impulse gradient modified from G to $G - \rho V$. Then, since the horizontal impulse on a fixed body is $I_x = Gk$, the horizontal impulse on the same body, but which is free to move, is the integral of P_1 over its surface:

$$I_{Vx} = (G - \rho V)k + \rho V\mathscr{V}. \tag{28}$$

We can then use any of Eqs. (24)–(27) to express k in whichever way is most natural.

Equating the impulse on the moving body B, of density ρ_B, with the change in momentum, $\rho_B\mathscr{V}V$, gives

$$V = \frac{Gk}{\rho_B\mathscr{V} + \rho(k - \mathscr{V})}. \tag{29}$$

With Eq. (27), this shows that V is independent of the size of B. Note that a more dense body moves less quickly. If the body moves, then the impulse on it is

$$I_{Vx} = \frac{G\rho_B\mathscr{V}k}{\rho_B\mathscr{V} + \rho(k - \mathscr{V})} \tag{30}$$

which is less than the impulse on a fixed body, since $k > \mathscr{V}$ by Eq. (27). (If $\lambda_x = 0$ then the impulse is zero.)

The horizontal force pushing a body, B, which is free to move, away from the wall when the wave breaks is the impulsive force, $F_\mathrm{I} = I_{Vx}/\Delta t$. In the opposite direction, friction, F_F, and the fluid drag force, F_D, resist the motion. We write $F_\mathrm{F} = \mu(\rho_B - \rho)\mathscr{V}g$, where μ is the coefficient of friction between B and the bed, and $F_\mathrm{D} = (1/2)\rho C_\mathrm{D}u_0^2\mathscr{A}$, where $\mathscr{A}$ is the cross-sectional area of the body in the direction of motion. C_D is a drag coefficient at approximately constant flow speed (appropriate to the body and Reynolds number) which Batchelor [19, Section 5.11] discusses for a circular cylinder and a sphere. For flows with Reynolds number 10^6, he gives $C_\mathrm{D} \approx 0.5$ for a circular cylinder and $C_\mathrm{D} \approx 0.2$ for a sphere. Then, comparing these forces acting on B shows that for B to move we must have

$$\frac{I_{Vx}}{\Delta t} > \mu(\rho_B - \rho)\mathscr{V}g + \frac{1}{2}\rho C_\mathrm{D}\mathscr{A}u_0^2. \tag{31}$$

Using Eqs. (27) and (30) gives the condition

$$\frac{\mathscr{V}}{\mathscr{A}} > \frac{(1/2)\rho C_\mathrm{D}u_0^2\Delta t(\rho_B + \rho\lambda_x)}{G\rho_B(\lambda_x + 1) - \mu(\rho_B - \rho)g\Delta t(\rho_B + \rho\lambda_x)} \tag{32}$$

for B to move. Since $\mathscr{V}/\mathscr{A}$ is proportional to the length scale of the body, this gives a lower bound for the critical length scale, a_c, at which a body will move. So if a body of given

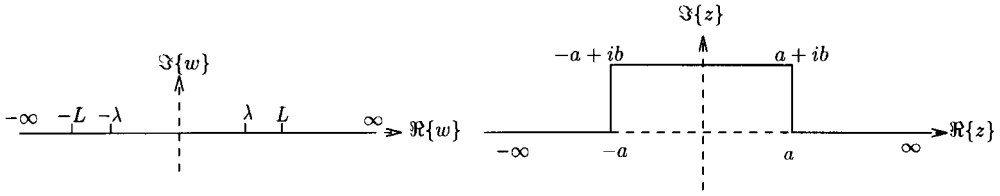

Fig. 3. Illustrating the construction of the conformal map for a rectangle on the sea bed. The map sends $\pm\infty \mapsto \pm\infty$, $\pm L \mapsto \pm a$ and $\pm\lambda \mapsto \pm a + ib$.

shape is large enough, it will move due to a nearby wave impact.

3.4. A body protruding from the wall

Since the normal derivative of the pressure impulse is zero on the wall, below the impact zone, this theory can also be used to find the effect of a wave impact on an object protruding from the wall. Considering again the contours of pressure impulse in Fig. 1 we see that a small body attached to the wall at a position $(0, -y_0)$, where $y_0 > 0.5\ H$, is subjected to a pressure impulse gradient down the wall. For a body whose size is much less than the height of the wall, we can approximate the gradient to be almost uniform, so that we are able to write the far field condition as $P \sim P_0 - Gx'$, where x' is now a coordinate pointing down the wall. Now $G = -\partial P_1/\partial x'|_{x=0,y=-y_0}$ and $P_0 = P_1|_{x=0,y=-y_0}$. The gradient, G, is evidently large, since the contours are so close together, and will act in such a way as to attempt to push the body towards the sea bed. We can again use a conformal map to represent the body, B, and, since the boundary conditions are the same as for the problem considered above, all the results transfer to this situation. Then the impulse on this body protruding from the wall has components I_x downwards (in the x' direction) and I_y pointing perpendicularly away from the wall.

We are also able to model the effect of the wave impact on a body that pierces the free surface at the instant of impact. In this region the pressure impulse gradient is perpendicular to the free surface, and will give an impulsive lift to the body. With the condition that $P = 0$ on the free surface we can adapt the results for some of the bodies on the sea bed using arguments based on symmetry. Note however, that the relevant value of G will change (as calculated from Fig. 1) and that we shall have $P_0 = 0$.

4. Results

We now give some examples of shapes for which the impulse is calculable, even if the distorted pressure impulse field is not. This allows Eq. (32) to be applied in order to decide how large a body on the sea floor must be for the impulsive forces to dominate and move the body. (We shall also correct some errors of Cooker and Peregrine [15]).

4.1. Semicircular cylinder

We find the impulse on a semicircular cylinder aligned with its axis parallel to the wall. A semicircle of radius a on the sea bed has added mass coefficient $\lambda_x = 1$ and area $\mathscr{V} = (1/2)\pi a^2$ so that Eq. (27) predicts

$$I_x = \pi G a^2. \tag{33}$$

This corrects the fallacious solution of Cooker and Peregrine [15, Eq. (4.13)]. Since $k = \pi a^2$, if the cylinder is free to move then its initial speed will be given by Eq. (29):

$$V = \frac{2G}{\rho_B + \rho}. \tag{34}$$

Note that this velocity is independent of the radius, a, of the cylinder.

The cross-sectional area (per unit length) in the direction of motion is $\mathscr{A} = a$. We take $\Delta t = 0.04$ s, $\mu = 0.5$, $\rho_B = 3\rho$, $C_D = 0.5$ and, for a water depth at the wall of $H = 10$ m, $u_0 = \sqrt{gH} = 9.91\ \mathrm{m\ s^{-1}}$. Then our estimate of the pressure impulse gradient is $G = 991\ \mathrm{N\ s\ m^{-3}}$. If its density is $\rho_B = 3\rho = 3 \times 10^3\ \mathrm{kg\ m^{-3}}$ then a semicircular cylinder will have an initial speed of $V = 0.496\ \mathrm{m\ s^{-1}}$. For the impulsive force on the semicircle to overcome the frictional and drag forces and move it, Eq. (32) implies that the critical value of a for the body to move is $a_c = 0.575$ m. Thus, a semicircular cylinder of radius $a > a_c$ is likely to be moved by the impact of this storm wave.

4.2. Circular cylinder

For a circular cylinder (or log) on the bed, lying parallel to the wall, the added mass coefficient is $\lambda_x = (1/3)\pi^2 - 1$ [20]. Then the horizontal impulse is

$$I_x = \frac{1}{3}\pi^3 G a^2. \tag{35}$$

The vertical impulse on the cylinder is zero, by Eq. (16), not the incorrect value reported by Cooker and Peregrine [15].

In order to find out if the impulsive force on the circle is likely to overcome the frictional and drag forces and move it, we apply Eq. (32). The area of the circle is $\mathscr{V} = \pi a^2$ and the cross-sectional area (per unit length) in the direction of motion is $\mathscr{A} = 2a$. Then, with the same parameters as in Section 4.1, we find that for the body to move $a_c = 0.5$ m. Thus, a circular cylinder of radius $a > a_c$ is likely to be moved by the impact of a storm wave.

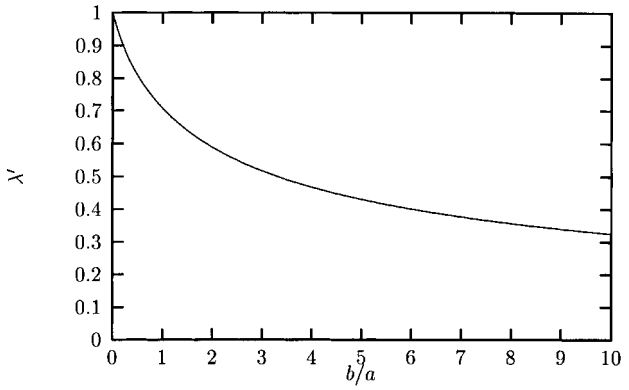

Fig. 4. A graph of the aspect ratio of the rectangle, b/a, against λ'. Note that as $\lambda' \to 0$, $b/a \to \infty$, corresponding to the vertical plate. Maple was used to evaluate Eq. (37) to provide the data for these curves.

4.3. Rectangular cylinder

Most structures near sea walls are made of rectangular blocks. To construct a rectangle on the sea floor, we apply the Schwarz–Christoffel mapping theorem to give the expression

$$\frac{\mathrm{d}z}{\mathrm{d}w} = \sqrt{\frac{w^2 - \lambda^2}{w^2 - L^2}} \tag{36}$$

where $\lambda \in [0, L]$ is a parameter governing the aspect ratio of the rectangle, which is at rest on the real axis with a vertical line of symmetry through the origin, as in Fig. 3. The map transforms the real line between $w = -L$ and L to the sides and top of a rectangle of width $2a$ and height b and transforms the remainder of the real w-axis to the real z-axis outside the rectangle. Note that $0 \le a, b \le L$, so that Eq. (36) can be used for any rectangle from a long flat plate, through a square, to a tall thin spike.

We let $\lambda' = \lambda/L$ then the half-width of this rectangle is

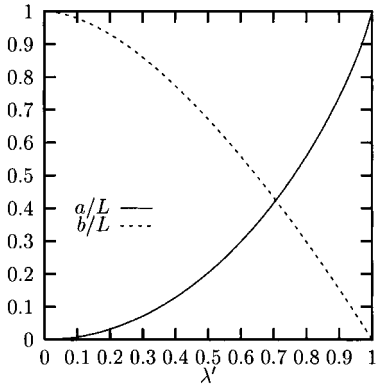

Fig. 5. A graph of the lengths of the sides of the rectangle, a/L and b/L, against λ'. Maple was used to evaluate Eq. (37) to provide the data for these curves.

given by

$$a = \int_0^{\lambda} \frac{\mathrm{d}z}{\mathrm{d}w}\mathrm{d}w = L\int_0^{\lambda'} \sqrt{\frac{\lambda'^2 - w^2}{1 - w^2}}\,\mathrm{d}w$$
$$= L\left\{\mathrm{E}\left(\frac{\pi}{2}, \lambda'\right) - (1 - \lambda'^2)\mathrm{F}\left(\frac{\pi}{2}, \lambda'\right)\right\}$$

(using Gradshteyn and Ryzhik [21, Eq. (3.169.10)]) where $\mathrm{F}(\phi, k)$ and $\mathrm{E}(\phi, k)$ are Incomplete Legendre Elliptic integrals of the first and second kinds respectively. The height is

$$b = \int_{\lambda}^{1} \frac{\mathrm{d}z}{\mathrm{d}w}\,\mathrm{d}w = L\int_{\lambda'}^{1} \sqrt{\frac{w^2 - \lambda'^2}{1 - w^2}}\,\mathrm{d}w$$
$$= L\left\{\mathrm{E}\left(\frac{\pi}{2}, \sqrt{1 - \lambda'^2}\right) - \lambda'^2\mathrm{F}\left(\frac{\pi}{2}, \sqrt{1 - \lambda'^2}\right)\right\}$$

(using Gradshteyn and Ryzhik [21, Eq. (3.169.12)]). Writing these in terms of Complete Elliptic integrals of the first and second kinds (K,E) and their associated Complete Elliptic integrals (K′,E′) (see Byrd and Friedman [22]) gives

$$a(\lambda') = L(\mathrm{E}(\lambda') - (1 - \lambda'^2)\mathrm{K}(\lambda')) \qquad \text{and}$$
$$b(\lambda') = L(\mathrm{E}'(\lambda') - \lambda'^2\mathrm{K}'(\lambda')). \tag{37}$$

It is not possible to relate λ explicitly to the dimensions of the rectangle. In practice one chooses an aspect ratio for the rectangle, b/a, from which a value of λ' can be found from Fig. 4. Then Fig. 5 enables a/L and b/L to be estimated, giving the size of the rectangle.

It is not possible to use Eq. (24) to find the horizontal impulse on this rectangle since we do not have an explicit conformal map, but the derivative of the conformal map. Neither do we know the added mass of the rectangle, so Eq. (26) cannot be applied. So, rather than integrating directly according to Eq. (14), we differentiate Eq. (19):

$$\frac{\mathrm{d}z}{\mathrm{d}w} = \sigma - \frac{b_1}{w^2} - \frac{2b_2}{w^3} - \cdots$$

then Eq. (24) implies

$$I_x = -\pi G\,\mathrm{R}(\sigma b_1) \tag{38}$$

where b_1 is now the coefficient of $-1/w^2$ in the expansion of $\mathrm{d}z/\mathrm{d}w$ for large w. For the rectangle, as $w \to \infty$ Eq. (36) becomes

$$\frac{\mathrm{d}z}{\mathrm{d}w} = \sqrt{\frac{w^2 - \lambda^2}{w^2 - L^2}} = \left(1 - \left(\frac{\lambda}{w}\right)^2\right)^{1/2}\left(1 - \left(\frac{L}{w}\right)^2\right)^{-1/2}$$
$$\sim 1 + \frac{1}{2w^2}(L^2 - \lambda^2) + \mathrm{O}\left(\frac{1}{w^4}\right).$$

Then $I_x = (\frac{1}{2})\pi G(L^2 - \lambda^2)$ and Eq. (26) predicts that the added mass of the rectangle for horizontal motion is

$$M_x = \rho\left(\frac{1}{2}\pi(L^2 - \lambda^2) - 2ab\right) \tag{39}$$

in agreement with the result of Barringer [23]. This predicts the special cases of the vertical plate of height $L(\lambda = 0)$ with horizontal impulse $(1/2)\pi GL^2$ and the identity transformation from the flat sea bed ($\lambda = L$) which receives zero horizontal impulse.

For a rectangle which is twice as wide as it is high, we have $b/a = 1$ and then $\lambda' = 1/\sqrt{2}$. Fig. 5 gives $a = b = 0.423L$, so we put $L = 1/0.423 = 2.361$ to give a rectangle of width 2 and unit height. For this rectangle the horizontal impulse is $I_x = 4.378G$. Thus for a rectangle of height c, width $2c$ and area $2c^2$ we have $I_x = 4.378Gc^2 = 2.189G(2c^2)$. This is much larger than the horizontal impulse of $I_x = 1.57Gc^2$ on a vertical plate of the same height, showing the effect of increasing width and area.

A square, with $b/a = 2$, has $\lambda = 0.588L$ by Fig. 4 and then $b = 2a = 0.570L$. If $L = 3.509$ then the square has side length 2 and $I_x = 12.653G$. So for a square of side length c the impulse is $I_x = 3.163Gc^2$. So the first rectangle, which is wide and low, receives a smaller horizontal impulse per unit cross-sectional area. Thus for a given cross-sectional area, the tallest rectangles receive the highest horizontal impulses, and rectangles with larger areas receive higher horizontal impulses.

4.4. Inclined plate

If a body is not left–right symmetric, then Eq. (15) gives a vertical component of impulse which is proportional to the pressure impulse gradient, G. For instance, the impulse can be computed on an inclined plate (whose cross-section is a straight line segment) of length a, projecting at an angle $\alpha \in (0, \pi)$ from the sea bed. The conformal map (adapted from Jeffrey [24]) is

$$z(w) = (w - a)^{\beta}\left(a + \frac{\beta w}{1-\beta}\right)^{1-\beta}$$

with $\beta = \alpha/\pi$. The plate lies between $z = 0$ and $z = (-1)^{\beta}a$ (taking the principle value) to which it is mapped from the real interval $[a(\beta - 1)/\beta, a]$ in the w plane. We have $z \sim \sigma w$ as $|z| \to \infty$, where $\sigma = (\beta/(1-\beta))^{1-\beta}$. Rearranging the conformal map for large w gives

$$z(w) = \sigma w\left(1 - \frac{a}{w}\right)^{\beta}\left(1 + \frac{a(1-\beta)}{\beta w}\right)^{1-\beta}$$

$$\sim \sigma w + \frac{a\sigma(1-2\beta)}{\beta} - \frac{a^2\sigma(1-\beta)}{2\beta w} + \mathrm{O}(w^{-2}).$$

Applying Eq. (24) gives the horizontal impulse

$$I_x = \frac{\pi G a^2 \sigma^2}{2}\left(\frac{1-\beta}{\beta}\right) = \frac{\pi G a^2}{2}\left(\frac{1-\beta}{\beta}\right)^{2\beta-1}. \qquad (40)$$

So the horizontal impulse is the same whether the plate leans to the right or to the left at a particular angle to the bed.

The total impulse, given by Eq. (15), is

$$\begin{aligned} I_x + \mathrm{i}I_y &= -\mathrm{i}G\sigma \int_{a(\beta-1)/\beta}^{a} z(u)\,\mathrm{d}u \\ &= -\mathrm{i}Ga^2\sigma \int_{(\beta-1)/\beta}^{1} (u-1)^{\beta}\left(1 + \frac{\beta}{1-\beta}u\right)^{1-\beta}\mathrm{d}u \\ &= -\mathrm{i}Ga^2\sigma(-1)^{\beta} \\ &\quad \times \left(\frac{\beta}{1-\beta}\right)^{1-\beta}\int_0^{1/\beta} x^{\beta}\left(\frac{1}{\beta} - x\right)^{1-\beta}\mathrm{d}x \\ &= -\frac{\mathrm{i}Ga^2\sigma}{2}\frac{(-1)^{\beta}}{\beta^2}\left(\frac{\beta}{1-\beta}\right)^{1-\beta}\Gamma(2-\beta)\Gamma(1+\beta) \\ &= -\frac{\mathrm{i}\pi Ga^2\sigma}{2}\left(\frac{1-\beta}{\beta}\right)^{\beta}\frac{(-1)^{\beta}}{\sin(\pi\beta)} \\ &= \frac{\pi Ga^2\sigma}{2}\left(\frac{1-\beta}{\beta}\right)^{\beta}(1 - \mathrm{i}\cot(\pi\beta)) \\ &= \frac{\pi Ga^2}{2}\left(\frac{1-\beta}{\beta}\right)^{2\beta-1}(1 - \mathrm{i}\cot(\pi\beta)) \end{aligned}$$

using Abramowitz and Stegun [25, Eq. (6.1.31)] and Gradshteyn and Ryzhik [21, Eq. (3.191)]. Then $I_y = -I_x\cot(\pi\beta)$ and for this asymmetric body the vertical component of impulse is non-zero. The impulse acts to push the plate either away from or towards the bed, depending on whether it leans to the left or the right respectively. Further calculation suggests that all asymmetric bodies on the sea bed will experience a component of impulsive lift perpendicular to the direction of the pressure impulse gradient, $G\hat{\mathbf{i}}$.

5. Sphere—a boulder on a beach

The case of a hemisphere on the sea bed is treated by Cooker and Peregrine [15]. If it has radius a and is fixed then the impulse on it is $I_x = \pi Ga^3$. Since $\lambda_x = 1/2$ for a sphere, Eq. (27) correctly predicts this value. So the added mass method of finding the horizontal impulse is valid for truly three-dimensional shapes too [26]. So now, for a sphere of radius a on the sea bed, the added mass coefficient is $\lambda_x = 0.621$ [27]. Then $I_x = 2.161\pi Ga^3$. If the sphere is free to move then its initial speed will be given by Eq. (29):

$$V = \frac{1.621G}{0.621\rho + \rho_{\mathrm{B}}}. \qquad (41)$$

If we think of the sphere as a boulder on a plane, gently sloping, beach, then this work may help to explain the sudden movement of bodies away from a wave impact on a shingle beach.

Shingle beaches may not constitute a large part of the coastal zone on a world-wide scale, but in Britain they are particularly prevalent. During storms, shingle is often

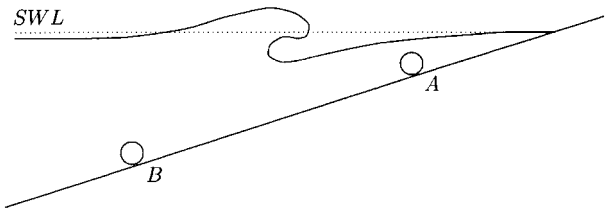

Fig. 6. The wave breaks close to the beach, causing a pressure impulse gradient to act up/down the beach above/below the impact, affecting the sphere in Case A/B respectively.

washed onshore so that beaches are steeper in winter. In the summer the generally smaller waves draw shingle away from the beach to offshore bars. Wave action on beaches also tends to grade beach material, pushing larger particles farther up the beach (landward). Further, coarser beach material gives steeper slopes of beach. When the beach material is a mixture of pebbles of different sizes, large particles move over the fine material and are thrown up on the shore [28]. Steers [29, p.14] gives data for pebble movement in moderate weather conditions on the north Norfolk coast. This shows daily pebble displacements of up to 72 yards, although the size of the pebbles is not specified.

The pressure impulse field after a wave impacts on a shingle beach is only slightly modified, by the presence of the shingle, from that for a flat sloping wall, in the same way that P is distorted only in a small localised region around a body on the sea bed. Typical values of beach slope are 6–10° [30,31]. Okamura [32] shows that the largest impulses occur when a wall is nearly vertical, but even for a wall at a very shallow angle we suggest that a breaking wave will still generate a large enough impulse to move a boulder on a beach. This is illustrated schematically in Fig. 6. The pressure impulse gradient points up the beach above the wave impact and points down the beach below. Each boulder responds to the local applied pressure gradient-if it is free to move it acquires some initial speed from the fluid impulse and is eventually brought to rest by friction with neighbouring bodies, gravity and fluid resistance. In this way a body is displaced a short distance by each wave impact. A succession of impacts in one place can lead to the movement by many small steps of beach material both up and down the beach away from the site of impact.

To avoid the problem of the wave impact being changed by the presence of the sphere on the shore, we assume that it is some distance away from where the impact occurs. Our aim is to follow the motion of one boulder, of density ρ_B, which is free to move. We assume that the boulder is spherical so its cross-sectional area is $\mathscr{A} = \pi a^2$ and its volume is $\mathscr{V} = (4/3)\pi a^3$. The beach is at an angle α to the horizontal and we assume that $\rho_B > \rho$, so that the sphere rests initially on the beach surface, immersed in fluid. (We do not take into account the possibility of the sphere leaving the beach surface throughout its motion, although this is possible for smaller bodies and larger impact pressures—compare with mechanisms for shingle beach formation and sorting in Cornish [33, Sections 4 and 5]). This surrounding fluid moves up the beach at speed u_0, due to the wave approaching the shore before impact, but will experience a change in velocity due to the impact of the wave. We expect u_0 to be about 10 m s^{-1}.

The complicated forces due to neighbouring boulders are modelled by a coefficient of friction, μ, between the sphere and the beach. If all the boulders on a beach were the same size, they would all be moved at similar velocities, so we assume that one boulder is larger than the average shingle size and that it projects above the level of the beach. Therefore μ is not prohibitively large. These forces on the sphere act at its centre of mass; we ignore any overturning moments and any rolling of the sphere down the beach. Thus our attention is restricted to the translational motion, as in the discussion in Section 3.1. The wet weight of the boulder is $W = (\rho_B - \rho)\mathscr{V}g$ and the frictional force is $F_F = \mu(\rho_B - \rho)\mathscr{V}g\cos\alpha$, where g is the acceleration due to gravity. The drag force from the fluid flowing at speed v_w over a sphere which moves at speed V is $F_D = (1/2)\rho\mathscr{A}C_D(v_w - V)^2$ where C_D is a drag coefficient. The directions of these forces are shown in Fig. 7. As before, we take $C_D = 0.2$ for a sphere in water moving at high Reynolds number.

After the impact the sphere moves with velocity V parallel to the beach, given by Eq. (41). The velocity component of the water parallel to the beach after impact is v_w, which differs from u_0 by an amount equal to G/ρ. This change in fluid velocity during impact is only about twice the initial speed of the sphere but we would expect the sphere to be rapidly brought to rest by the frictional forces.

Two cases are treated, which are illustrated in Fig. 7.

- Case A: The wave breaks below the sphere, which is initially pushed up the slope by the impact. The fluid

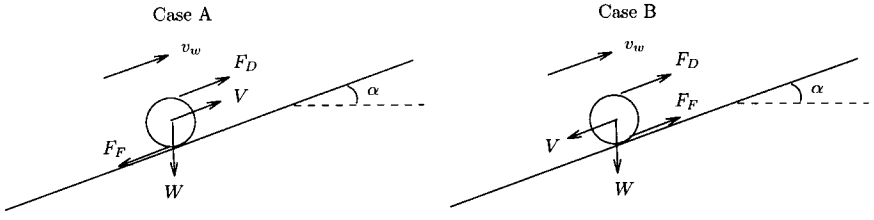

Fig. 7. The geometry for Cases A and B. In Case A the fluid flows up the beach, which is at an angle α to the horizontal, assisting the progress of the sphere, of weight $W = g(\rho_B - \rho)\mathscr{V}$, which moves at initial velocity V. In Case B the initial direction of motion of the sphere is down the beach. Friction opposes the motion in both cases, and the fluid drag acts up the beach.

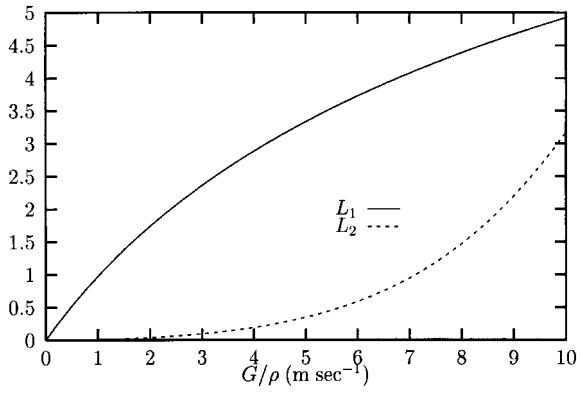

Fig. 8. The distances, in metres, moved up the beach, L_1, and down the beach, L_2, by the sphere before it first comes to rest as functions of the change in fluid velocity due to the wave impact, G/ρ. The parameters used are $\mu = 0.5$, $a = 0.2$ m, $g = 9.8$ m s^{-2}, $\rho_B/\rho = 3.0$, $\alpha = 10.0°$ and $C_D = 0.2$. This gives $K = 0.353$, $c_+ = 2.11$ and $c_- = 1.44$. The sphere is given an initial impulsive velocity of $V = 0.45G/\rho$. The spherical boulder can move about 5 m up the beach or 3 m down the beach.

which moved past the sphere at speed u_0 is accelerated to move up the beach at speed $v_w = u_0 + G/\rho$, helping to continue the upslope motion of the sphere by fluid drag. Friction and the weight of the sphere oppose the motion.

- Case B: The wave impacts farther up the beach than the sphere and the sphere is initially pushed down the slope by the wave impact. The water flows up the slope at speed $v_w = u_0 - G/\rho$, retarding the motion of the sphere by drag. In this case the weight of the boulder assists its motion down the slope.

Other combinations of the direction of the initial velocity and the water velocity can be modelled, but are almost equivalent, mathematically, to these two cases. The sphere's speed at time t is denoted by $V_i(t)$, where $i = 1,2$ denotes case A or B. Similarly, the distance that it moves before first coming to rest at time $t_i > 0$ (i.e. $V_i(t_i) = 0$) is L_i.

5.1. Case A

The breaking wave impacts to seaward of the sphere so that the impulse pushes it up the slope, with initial speed $V_1 = V$, and water flows over it, up the beach, with speed, $v_w = u_0 + G/\rho$. Thus the water's motion aids the sphere's motion up the beach. This is modelled by the ODE

$$K^2(v_w - V_1)^2 - c_+^2 = \frac{\mathrm{d}V_1}{\mathrm{d}t} \tag{42}$$

where

$$K^2 = \frac{1}{2}\frac{\rho \mathscr{A} C_D}{\rho_B \mathscr{V}} = \frac{3}{8}\frac{\rho C_D}{\rho_B a} \qquad \text{and}$$

$$c_+^2 = g\left(1 - \frac{\rho}{\rho_B}\right)(\mu\cos\alpha + \sin\alpha) > 0.$$

The first term on the left-hand side of Eq. (42) represents the drag forces and the second the frictional forces. Defining

$$\gamma_\pm = c_+ \pm K(v_w - V) \qquad \text{and} \qquad \beta_\pm = c_+ \pm K v_w$$

gives the solution to Eq. (42):

$$V_1(t) = v_w + \frac{c_+}{K}\left[\frac{\gamma_- \mathrm{e}^{-2c_+Kt} - \gamma_+}{\gamma_- \mathrm{e}^{-2c_+Kt} + \gamma_+}\right]. \tag{43}$$

The sphere comes to rest after a time

$$t_1 = \frac{1}{2Kc_+}\log\left|\frac{\gamma_+\beta_-}{\gamma_-\beta_+}\right| \tag{44}$$

having travelled a distance up the beach of

$$L_1 = \frac{v_w}{2Kc_+}\log\left|\frac{\gamma_+\beta_-}{\gamma_-\beta_+}\right| + \frac{1}{2K^2}\log\left|\frac{\beta_+\beta_-}{\gamma_+\gamma_-}\right|. \tag{45}$$

5.2. Case B

In this case the movement of the water retards the motion of the sphere. The wave has broken after passing landward of the sphere, so that the impulse acts in the seaward direction, whilst water is still passing over it up the beach with velocity $v_w = u_0 - G/\rho$. We solve

$$-K^2(v_w + V_2)^2 - c_-^2 = \frac{\mathrm{d}V_2}{\mathrm{d}t} \tag{46}$$

subject to $V_2(t = 0) = V$ and where

$$c_-^2 = g\left(1 - \frac{\rho}{\rho_B}\right)(\mu\cos\alpha - \sin\alpha) > 0$$

i.e. $\mu > \tan(\alpha)$ so that the sphere is held at rest by friction when there are no impulsive forces ($v_w = u_0$). K is as for Case A. We redefine

$$\gamma_\pm = \mathrm{i}c_- \pm K(v_w + V) \qquad \text{and} \qquad \beta_\pm = \mathrm{i}c_- \pm K v_w,$$

and then the sphere's velocity down the beach is given by

$$\begin{aligned} V_2(t) &= -v_w + \frac{c_-}{K}\tan\left[-c_-Kt + \tan^{-1}\left(\frac{K(v_w + V)}{c_-}\right)\right] \\ &= -v_w - \frac{c_-}{K}\left[\frac{\gamma_- \mathrm{e}^{-2\mathrm{i}c_-Kt} - \gamma_+}{\gamma_- \mathrm{e}^{-2\mathrm{i}c_+Kt} + \gamma_+}\right] \end{aligned} \tag{47}$$

and it comes to rest after a time

$$\begin{aligned} t_2 &= \frac{1}{Kc_-}\left[\tan^{-1}\left(\frac{K(v_w + V)}{c_-}\right) - \tan^{-1}\left(\frac{Kv_w}{c_-}\right)\right] \\ &= \frac{\mathrm{i}}{2Kc_-}\log\left(\frac{\gamma_+\beta_-}{\gamma_-\beta_+}\right) \end{aligned} \tag{48}$$

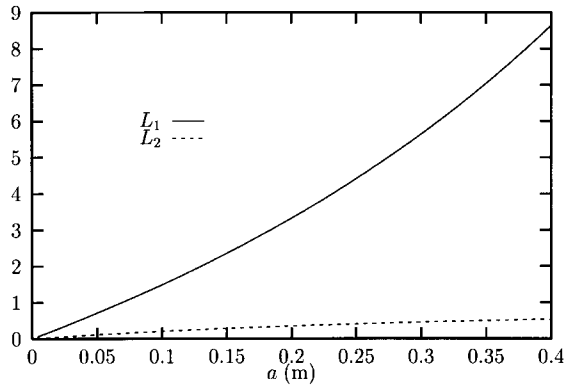

Fig. 9. The distances, in metres, moved up the beach, L_1, and down the beach, L_2, by the sphere before it first comes to rest, as functions of its radius a. The parameters used are $\mu = 0.5$, $g = 9.8\ \mathrm{m\,s^{-2}}$, $\rho_B/\rho = 3.0$, $\alpha = 10.0°$, $G/\rho = 5\ \mathrm{m\,s^{-1}}$ and $C_D = 0.2$. The sphere is given an initial impulsive velocity $V = 2.25\ \mathrm{m\,s^{-1}}$.

having moved a distance down the beach of

$$L_2 = \frac{1}{K^2}\log\left(\frac{\cos\left(\tan^{-1}\left(Kv_w/c_-\right)\right)}{\cos\left(\tan^{-1}\left(K(v_w+V)/c_-\right)\right)}\right) - v_w t_2$$
$$= \frac{1}{2K^2}\log\left(\frac{c_-^2 + K^2(v_w+V)^2}{c_-^2 + K^2 v_w^2}\right) - \frac{\mathrm{i}v_w}{2Kc_-}\log\left(\frac{\gamma_+\beta_-}{\gamma_-\beta_+}\right)$$
$$= -\frac{\mathrm{i}v_w}{2Kc_-}\log\left(\frac{\gamma_+\beta_-}{\gamma_-\beta_+}\right) - \frac{1}{2K^2}\log\left(\frac{\beta_+\beta_-}{\gamma_+\gamma_-}\right). \tag{49}$$

Note that, despite the presence of the complex number i, the quantities V_2, t_2 and L_2 are all real.

5.3. Results

The form of the solutions for V_i, t_i and L_i are similar for $i = 1,2$. Fig. 8 shows the distance that the sphere moves for each of the two cases, L_1 and L_2, as a function of G/ρ, the change in velocity of the water flowing over the sphere due to the wave impact. The sphere of radius $a = 0.2$ m is set into motion by the wave impact. It has density $\rho_B = 3\rho$ so that its initial velocity is $V = 0.45G/\rho$. In Case A the sphere moves a large distance even for small changes in water velocity, showing how the fluid drag assists its progress. As G/ρ increases the initial velocity of the sphere is a higher fraction of the fluid velocity, so that this drag effect decreases and the gradient of the graph decreases. For a change in fluid speed of $G/\rho = 10\ \mathrm{m\,s^{-1}}$, the boulder moves almost 5 m up the beach. This is associated with a value of the impulsive pressure gradient of $G = 10^4\ \mathrm{N\,s\,m^{-3}}$, which is over ten times larger than the gradients along the sea floor hypothesised earlier. In Case B the boulder moves only short distances for changes in water velocity of up to $5\ \mathrm{m\,s^{-1}}$, due to the high fluid drag up the beach. However, at $G/\rho = 10\ \mathrm{m\,s^{-1}}$ the fluid is brought to rest around the sphere and it travels about 3 m down the beach. For Case A, increasing ρ_B or μ both act to decrease L_1. In contrast, increasing ρ_B or decreasing μ will increase L_2.

Fig. 9 shows that as the radius of the sphere, a, increases, the distance moved either up or down the beach increases. Again, a boulder will move farther up than down the beach. This may explain the observation that larger boulders collect at the top of the beach or offshore on bars. Also, boulders will move farther up the beach than down, so that a boulder is more likely to be thrown up on the shore. Note that the water only flows up the beach for a short time, then recedes before the next wave breaks, so that in practice the sphere is likely to come to rest before being moved by the next impact event. During a storm there may be hundreds of wave impacts generating impulsive pressures and, collectively, pushing bodies considerable distances.

The L_i, $i = 1,2$ represent the distance travelled by a sphere on an inclined plane beach. We define an angle β that the incoming wave makes with the line of steepest ascent up the beach, and a coordinate system **i**,**j**,**k** where **i** points landward, **j** along the shoreline and **k** vertically upward. Then the direction in which the sphere moves on the plane of the beach (assuming that it moves in short straight jumps) is

$$\mathbf{L}_i = L_i(\cos\beta\cos\alpha\mathbf{i} + \sin\beta\mathbf{j} + \cos\beta\sin\alpha\mathbf{k}), \qquad i = 1,2.$$

Thus, given the angle of incidence of waves on a beach, it is possible to follow the process of what Palmer [31] calls progression, where a boulder is moved up and along the beach. A boulder will be pushed in the direction of $\mathbf{L}_i$ until coming to rest after a distance L_i and will then be dragged seaward, down the line of steepest descent by the backwash, this latter motion generally being shorter, particularly for larger bodies.

6. Conclusions

It has been shown that when a wave breaks against a plane impermeable surface, there are large pressure gradients acting within the fluid. The gradient, G, of the pressure impulse, $P = \int_{t_b}^{t_a} p\,\mathrm{d}t$, causes an impulsive force to act on a body. If, for a wave of height 10 m, the body has radius greater than about half a metre, this impulsive force will overcome the frictional forces that normally hold such a body in place. We find that for a given volume, tall thin cylindrical objects on the sea bed receive large impulses compared to low, wide ones and are therefore the shapes of body that we expect to be moved the farthest. These impulses, and the related velocity of a body that is free to move, can be calculated using the added mass and the volume of the body. The velocity of the body depends only on its shape, and not its size.

This analysis extends also to truly three-dimensional objects on the sea bed, and in particular we approximate a blunt, amorphous boulder on a shingle beach by a sphere. The impulsive force acting on a sphere on an inclined beach

is compared with the frictional and drag forces which normally act on a body to anchor it to the sea bed. The fluid drag force assists a boulder in moving up the slope of the beach, so that large boulders can be moved considerable distances. Moreover, larger boulders are moved farther by the effects of wave impact, so that they will collect towards the top or bottom of a beach, rather than in the surf zone. This accords with observations of the motion of large objects on shingle beaches.

Acknowledgements

The authors wish to thank the referees for their assistance. SJC acknowledges financial support from both the School of Mathematics at the University of East Anglia and the UK Engineering and Physical Sciences Research Council, award number 96000215.

References

[1] Tanimoto K, Takahashi S. Japanese experiences on composite breakwaters. In: Proceedings of the International Workshop on Wave Barriers in Deepwaters, Port and Harbour Research Institute, Japan, 1994. pp. 1–22.
[2] Hitachi S. Case study of breakwater damages—Mutsu-Ogawara Port. In: Proceedings of the International Workshop on Wave Barriers in Deepwaters, Port and Harbour Research Institute, Japan, 1994. pp. 308–29.
[3] Hattori M, Arami A, Yui T. Wave impact pressures on vertical walls under breaking waves of various types. Coastal Engng 1994;22:79–114.
[4] Blackmore PA, Hewson PJ. Experiments on full-scale wave impact pressures. Coastal Engng 1984;8:331–346.
[5] Chan ES, Melville WK. Deep-water plunging wave pressures on a vertical plane wall. Proc Roy Soc London A 1988;417:95–131.
[6] Bagnold RA. Interim report on wave-pressure research. J Inst Civil Engng 1939;12:201–226.
[7] Baird WF, Caldwell JM, Edge WL, Magoon OT, Treadwell DD. Report on the damages to the Sines breakwater, Portugal. In: Proceedings of the 17th International Conference on Coastal Engineering, ASCE Sydney, Australia, 1980. pp. 3063–77.
[8] Cunningham B. Harbour engineering. London: C. Griffin, 1928.
[9] Gaillard DD. Wave action in relation to engineering structures. Washington DC: US Government Printing Office, 1904.
[10] Stevenson T. The design and construction of harbours. Edinburgh: Black, 1864.
[11] Stevenson T. Account of experiments upon the force of the waves of the Atlantic and German Oceans. Trans Roy Soc Edinburgh 1849;16:23–32.
[12] Grilli ST, Losada MA, Martin F. Wave impact forces on mixed break-waters. In: Proceedings of the 23rd International Conference on Coastal Engineering, ASCE Venice, Italy, 1992. pp. 1161–74.
[13] Müller G. Wave impact pressures on a vertical wall and their effect on sea bed pressures. In: Proceedings of the XXVI IAHR Congress, vol. 3, 1995. pp. 275–80.
[14] Cooker MJ, Peregrine DH. Pressure-impulse theory for liquid impact problems. J Fluid Mech 1995;297:193–214.
[15] Cooker MJ, Peregrine DH. Wave impact pressure and its effect upon bodies lying on the sea bed. Coastal Engng 1992;18:205–229.
[16] Kober H. A dictionary of conformal representations. New York: Dover, 1957.
[17] Pólya G. A minimum problem about the motion of a solid through a fluid. Proc Natl Acad Sci 1947;33:218–221.
[18] Newman JN. Marine hydrodynamics. Cambridge, MA: MIT Press, 1978.
[19] Batchelor GK. An introduction to fluid mechanics. Cambridge: Cambridge University Press, 1973.
[20] Greenhow M, Yanbao L. Added masses for circular cylinders near or penetrating fluid boundaries-review, extension and application to water-entry, -exit and slamming. Ocean Engng 1987;14(4):325–348.
[21] Gradshteyn IS, Ryzhik IM. In: Jeffrey A, editor. Table of integrals, series and products, 5th ed. New York: Academic Press, 1965.
[22] Byrd PF, Friedman MD. Handbook of elliptic integrals. Berlin: Springer, 1971.
[23] Barringer IE. The hydrodynamics of ship sections entering and exiting a fluid. PhD thesis, Department of Mathematics and Statistics, Brunel University, 1998.
[24] Jeffrey A. Complex analysis and applications. London: CRC, 1992.
[25] Abramowitz M, Stegun IA. Handbook of mathematical functions. New York: Dover, 1965.
[26] Cox SJ. Pressure impulses caused by wave impact. PhD thesis, School of Mathematics, University of East Anglia, 1998.
[27] Davis AMJ. High frequency limiting virtual-mass coefficients of heaving half-immersed spheres. J Fluid Mech 1977;80:305–319.
[28] Zenkovich VP. Processes of coastal development. London: Oliver and Boyd, 1967.
[29] Steers JA. The sea coast. London: Collins, 1953.
[30] Caldwell NE, Williams AT. Spatial and seasonal pebble beach profile characteristics. Geol J 1986;21(2):127–138.
[31] Palmer HR. Observations on the motions of shingle beaches. Phil Trans Roy Soc London 1834;124:567–576.
[32] Okamura M. Impulsive pressure due to wave impact on an inclined plane wall. Fluid Dyn Res 1993;12(4):215–228.
[33] Cornish V. On sea-beaches and sandbanks. Geogr J 1898;11:528–543. See also pp. 628–51.